High Temperature Creep Behaviour in the γ titanium aluminide Ti-45Al-2Mn-2Nb

Z. Abdallah, M.T. Whittaker, M.R. Bache

Institute of Structural Materials, College of Engineering, Swansea University, Singleton Park, Swansea, SA2 8PP, UK.

Abstract

The fact that Gamma titanium aluminides (γ-TiAl) offer strong potential for replacing conventional titanium and nickel-base alloys in future gas turbine engine designs has resulted in the requirement to accurately describe the creep behaviour of these complex alloys. Consequently, the system Ti-45Al-2Mn-2Nb has been extensively studied under high temperature creep conditions where creep ductilities are shown to far exceed the relatively low tensile ductilities characteristic of the alloy at room temperature. Modern lifing approaches have been applied to the alloy, helping to develop understanding of the deformation behaviour, and are shown to accurately describe the stress-rupture and minimum creep rate behaviour of the alloy, promoting confidence for the derivation of computational models which are used to describe the behaviour of the alloy for in service conditions. When compared to an existing, conventional, high temperature titanium alloy, Timetal 834, significant improvements in creep life were demonstrated for equivalent stress conditions with a comparable level of creep ductility between the two alloys. In addition, the gamma titanium aluminide showed a superior resistance to surface oxidation and associated cracking with notable α case formation in Timetal 834 leading to premature failure.

Keywords

A. Titanium aluminides, A. Intermetallics, B. Creep, G. Aero-engine components, B. Oxidation.

1. Introduction

For engineering applications where weight reduction, improved fuel consumption and high efficiency are essential requirements, titanium aluminide alloys warrant consideration due to their attractive balance of properties. Of particular value to gas turbine designers are their low density (approximately half of that of nickel-base alloys) as well as their high temperature capabilities (especially at temperatures which exceed the capability of conventional titanium alloys) resulting in a higher combustion efficiency and thus, fuel savings [1]. In general, titanium aluminide alloys are either classified as alpha-2 Ti_3Al or γ TiAl according to their composition and microstructural evolution [2, 3]. Amongst these, γ TiAl has received the greatest attention and showed a great potential as a material of considerable importance in the aerospace industry. This is because it shares with conventional titanium alloys the properties of low density, good corrosion resistance and high temperature capability. In particular, γ TiAl offers an increased resistance to creep and a superior oxidation resistance at very high temperatures [2]. This offers an advantage in

applications where temperatures exceed 600^{o}C, at which temperature the mechanical strength and creep behaviour of conventional titanium alloys become inadequate and oxidation problems arise due to the formation of a brittle oxidised surface layer (alpha-case), which leads to premature damage and fracture [4]. However, the poor ductility of gamma aluminides at low and intermediate temperatures, together with low fracture toughness and high rates of crack propagation, remain the major concerns for the employment of these alloys in engineering structures. Therefore, continued research is required to understand and predict their mechanical behaviour [2, 4]. Extensive research has taken place over the past three decades to optimise intermetallic alloys with an acceptable level of ductility. The first significant advance was achieved by introducing elements that stabilise the β phase to attain reasonable levels of ambient temperature ductility, through the addition of niobium (Nb), which provided an attractive combination of a superior creep and oxidation resistant alloys compared with conventional titanium alloys [2, 5]. At the same time, the addition of manganese (Mn) has also resulted in an improvement in the room temperature ductility [6]. Based on these findings, focus has been placed on alloys with an equivalent aluminium content ranging between 45 and 50%, with the system Ti-45Al-2Mn-2Nb, with a fully lamellar microstructure, proving to be of particular interest [7]. After a comprehensive programme of laboratory study, this paper will report a fundamental creep assessment conducted on the alloy, Ti-45Al-2Mn-2Nb, along with a comparison to results from the conventional titanium alloy, Timetal 834.

Furthermore, the paper seeks to address the creep performance of these alloys in the light of new approaches to creep lifing behaviour. The Wilshire equations have been successful in describing stress rupture behaviour for a range of alloys [8-11], and particularly in extrapolation of short term data to long life prediction. They seek to offer a coherent, holistic view of creep deformation and offer useful insights in comparison to more established techniques such as the Larson-Miller approach, also utilised in the current paper. Clearly the requirement of these techniques is primarily to accurately describe the stress-rupture behaviour of the material in question, in order to provide an accurate methodology for various computational approaches. As such, a further technique, the hyperbolic tangent approach, developed by Rolls-Royce plc, is also considered in order to allow for comparisons between modern methodologies.

2. Experimental Procedures

The Ti-45Al-2Mn-2Nb alloy was supplied in the form of cast and HIP'ed bars with a fully lamellar microstructure, Figure 1. This microstructural form is consistent with previously reported studies [12, 13]. Creep specimens were machined from the bar stock material. The gauge section was ground finished to a diameter of 5.6mm while the gauge length, as defined by the distance between the two circumferential "pips" used for the attachment of high precision extensometry, was 28.0mm. Creep specimens were tested under tension in air according to the international standard ISO 204 but using machines that apply a constant-stress condition throughout the course of the test. Test temperatures varied between 625-750^{o}C under selected applied stress levels between 150 and 550MPa. Each specimen was heated using a three-zone furnace and the temperature was monitored along the gauge length using calibrated type-R thermocouples in contact with the specimen surface. The creep elongation was measured using a parallel extensometer cage system clamped to the

"pips" of the gauge section and monitored using two high precision LVDTs. Full details of the Swansea based equipment and test techniques have been previously reported [14]. Following each creep test, examination of the deformed specimen was carried out using a JEOL 6100 Scanning Electron Microscope (SEM). Metallographic sections were then prepared on a plane orthogonal to the fracture surface, etched using a solution of H_2O (25ml) + HNO_3 (25ml) + HF (2ml) + glycerine (50ml) in order for the microstructure to be revealed [13, 15] and examined under optical microscopes

3. Results

3.1 Creep Behaviour

For the Ti-45Al-2Mn-2Nb alloy, full creep curves, i.e. creep strain, ε, against time, t, were obtained for all tests, an example of which is shown in Figure 2. From these curves, the time at which each specimen fractured, t_f, and the creep strain at fracture, ε_f, (generally called the creep ductility) were defined. The slope at any point on this curve ($\dot{\varepsilon} = d\varepsilon/dt$) represents the instantaneous strain rate. These creep curves would traditionally be described as showing classical creep behaviour characterised by three successive stages, namely: primary, secondary and a tertiary stage which, eventually, ends at rupture. However, more recent approaches [16] suggest that these curves may be more aptly described as a decaying primary phase followed by an accelerating tertiary phase, which results in a minimum, not steady state, creep rate. As expected from classical creep theories, the creep life, t_f, was found to decrease with increasing stress, σ (at constant temperature) or increasing temperature, T (at constant stress) in agreement with the power law equation [14]:

$$1/t_f \propto \dot{\varepsilon}_m = A\,\sigma^n \exp(-Q_c/RT) \qquad \text{.....(1)}$$

where A is a material constant, n is the stress exponent, Q_c is the minimum amount of energy required to initiate creep (activation energy) and R is the gas constant (8.314 J/mol K).

The value of the stress exponent, n, for this alloy was calculated by plotting $\ln(\sigma)$ against $\ln(\dot{\varepsilon}_m)$ at constant temperatures, as shown in Figure 3, where the slope of each trend line represents the value of n for that specific temperature. As obtained in previous studies on different materials [17], it is evident that the value of n varied between 5 and ~ 7 in the temperature range 675-750^{o}C (lower stress regime) whereas it increased from 8 up to ~ 11 in the temperature range 625-650^{o}C (higher stress regime). Based on traditional approaches, n values > 4 would be thought to indicate dislocation creep as the prevalent creep mechanism. Similarly, the activation energy (Q_c) for this alloy can be calculated by plotting ($1/T$) against $\ln(t_f)$ at constant stress values, Figure 4, where the slope of each line represents the activation energy at that temperature. From this figure, as with the value of the 'constant' n, a significant variation in the value of the activation energy was found (ranging from ~ 255 to ~ 520 kJ/mol K). For this reason, the variability of these 'constants' restricts the use of the power law equation for obtaining reliable properties through extrapolation. Therefore, alternative approaches were sought to describe the creep performance of the TiAl material. It is worthwhile mentioning that the left-hand side of equation (1), i.e. $1/t_f \propto \dot{\varepsilon}_m$, known as the Monkman-Grant relation [18], suggests that

the time to fracture, t_f, is inversely proportional to the minimum creep rate, $\dot{\varepsilon}_m$. This has been confirmed for the Ti-45Al-2Mn-2Nb alloy, as illustrated in Figure 5, with a Monkman-Grant constant equal to 0.1041.

3.2 Stress-Rupture Behaviour

The general stress dependence of the creep life of the alloy Ti-45Al-2Mn-2Nb was obtained by plotting the time to fracture values, t_f, recorded over a relatively wide temperature range against stress providing a stress rupture plot, as shown in Figure 6. This plot is in agreement with equation (1) wherein the time to fracture decreases with increasing stress level (at a constant temperature). Similarly, when selecting a constant stress value, the time to fracture decreases with increasing temperature. Whilst suitable fits can be made to the data using the least squares method, it is beneficial to be able to utilise a methodology which can be applied predictively to the current data. Many parametric methods have been proposed in order to describe creep behaviour, including numerous models for the prediction of long term creep properties based only on short-term measurements. Traditional methods such as the Larson-Miller or Manson-Haferd parameters have been shown to be deficient in this requirement, whereas more recent techniques such as the Wilshire equations show significant promise. Although aero-engine applications do not invoke a prediction of long-term creep behaviour, since components are not designed to operate into such regimes, a number of lifing methodologies have been considered purely on their ability to accurately describe the stress-rupture behaviour of the alloy across mid-term lifetimes.

3.2.1 The Wilshire Equations for Life Prediction

The Wilshire technique is mainly based on normalising the stress, σ, through the ultimate tensile strength, σ_{TS}, and eliminating the dependence of the activation energy on temperature (which under previous models caused the value of Q_c in the power law to vary) [8, 9]. Hence, equation (1) can be re-written as:

$$\dot{\varepsilon}_m = A^* (\sigma/\sigma_{TS})^n \exp(-Q_c^*/RT) \qquad \text{.....(2)}$$

where $A^* \neq A$ and $Q_c^* \neq Q_c$. The value of Q_c* for the alloy Ti-45Al-2Mn-2Nb was calculated as 330kJ/mol K. However, the value of the exponent n potentially remains variable, hindering the potential for prediction. Based on equation (2), the stress and temperature dependences are described by the Wilshire equation as [10-11]:

$$\sigma/\sigma_{TS} = \exp(-k_1 [t_f \exp(-Q_c^*/RT)]^u) \qquad \text{.....(3)}$$

where the value of k_1 and u are constants and can be obtained by following the same approach previously suggested in other studies [10-11] as shown in Figure 7. It is clear from this plot that the data set was bi-modal, giving two distinct linear regimes, namely the high and the low stress regimes. Based on this, different values of k_1 and u were obtained for the two regimes. Inserting these values into equation (3) provides the stress rupture curves, shown in Figure 8, over broad stress ranges

at selected temperatures. It is clear that the Wilshire predictions accurately describe the creep rupture behaviour under all test conditions.

3.2.2 Hyperbolic Tangent Predictions

The hyperbolic tangent technique was developed by staff based at Rolls-Royce plc in the 1990s for the purpose of creep lifing predictions. It implies that the highest stress that can be applied on a specified material is the ultimate tensile strength of that material, σ_{TS}, at any given temperature. This mirrors the Wilshire approach where the curves in Figure 8 intersect with the stress axis at a value equal to σ_{TS} when t = 0. The stress rupture behaviour described by the hyperbolic tangent technique over a wide range of temperatures is given by [19-21]:

$$\sigma = \sigma_{TS} / 2 \{1 - \tanh [k \ln (t / t_i)]\} \quad \text{.....(4)}$$

where k and t_i are fitting parameters that can be obtained by regression analysis using the experimental data at each temperature. Once the values of k and t_i are obtained, they can be inserted into equation (4) to produce the stress rupture predictive curves, as shown in Figure 9. It can be seen from this graph that the hyperbolic tangent method provided a reasonable fit to the Ti-45Al-2Mn-2Nb stress rupture data. The only limitation is that the inflection points found in these predictive curves have no theoretical explanation [21].

3.2.3 The Larson-Miller Equation's Predictions

This parametric approach is one of the methods traditionally used to predict the stress rupture data of metals. It was originally derived from the power law (equation 1) at a constant σ but a variable value of T and Q_c, which gave the final form of the Larson-Miller equation as [22]:

$$P_{LM} = f(\sigma) = T (C_{LM} + \log t_f) \quad \text{.....(5)}$$

where C_{LM} and P_{LM} are the Larson-Miller constant and parameter, respectively. The value of P_{LM} and C_{LM} can be obtained by plotting $\ln(t_f)$ against $1/T$ at constant stress values where the slope of the resulted lines represents the value of P_{LM} whereas the intercept is the value of C_{LM}. For the alloy Ti-45Al-2Mn-2Nb, the average value of the Larson-Miller constant, C_{LM}, was ~ 29. This value is in stark contrast to the original suggestion of Larson and Miller who assumed that the value of this constant should be always taken as 20 [19]. Based on this analysis, the stress-time prediction curves were constructed as shown in Figure 10. It can be observed that the Larson-Miller approach provides relatively poor fits at the low and intermediate temperatures whereas the correlation improved for temperatures above 700^{o}C.

3.3 Minimum Creep Rate Properties

The stress and temperature dependencies of the minimum creep rate, $\dot{\varepsilon}_m$, can be described using the second form of the Wilshire technique [10, 11, 23]:

$$\sigma/\sigma_{TS} = \exp\left(-k_2 \left[\dot{\varepsilon}_m \exp\left(Q_c^*/RT\right)\right]^v\right) \qquad \text{.....(6)}$$

where the value of k_2 and v can also be obtained by adopting a similar procedure [10, 11, 23]. Again, this data set indicated a bi-modal relationship resulting in different values of k_2 and v for the high and the low stress regimes, as illustrated in Figure 11. These values were then inserted into equation (6) producing the Wilshire prediction curves, as plotted in Figure 12. The Wilshire curves demonstrated an impressive description of the minimum creep rate behaviour of this alloy.

4. Discussion

In attempting to understand the creep behaviour of the γ TiAl alloy studied here, it is important to remember that one of the features of this alloy which limits its applications is its inherent brittle nature, with tensile ductilities at room temperature typically 1-2% [24]. It is interesting, therefore, to consider the ductility measured under elevated temperature creep testing (i.e. the strain at failure, ε_f), Figure 13. Even for relatively low temperatures such as 625°C, ductilities exceeding 15% were regularly measured, increasing to approximately 30% at the higher range of assessment. This could be attributed to an increase in vacancy concentration with temperature [25, 26]. A survey of the literature showed that there are several studies on the creep resistance of the lamellar alloys in which it was proved that the fully lamellar microstructure provides an optimum creep resistance [27]. In addition, a further study [28] showed that improved creep resistance of the fully lamellar structure has been attributed to a reduced lamellar spacing (~ 3µm). This was related to the restricted generation of dislocations within the material with the reduced lamellar interfaces, as these interfaces are found to be the major sources for dislocations [28].

An example of creep failure in γ-TiAl specimens is shown in Figure 14 (a), where the significant reduction in area is evident. Figure 14 (b) illustrates the relatively flat fracture plane, consisting of interlamellar and intergranular cracking, and immediately flanked by subsidiary surface cracking formed exclusively within the neck region. The lack of cracking at locations away from the neck was confirmed via orthogonal metallographic sectioning. This is shown in Figure 14 (c) and (d) wherein it is evident that interlamellar cracking took place along the interlamellar interfaces. The lack of surface cracking confirms the theory that creep failure was mostly occurring internally as a result of voids growing along the interlamellar interfaces. The significant degree of creep ductility at elevated temperatures enhances the potential of the alloy for gas turbine applications. In fact, it is instructive to compare the creep performance of this alloy with that of a conventional alloy, namely Ti834 (Ti-5.8Al-4Sn-3.5Zr-0.7Nb-0.5Mo-0.35Si-0.06C). Ti834 is widely used in the compressor sections of the gas turbine engine and essentially represented the culmination of extensive research during the 1980s to design (α+β) alloys capable of operating at increased temperatures.

Figure 15 shows a comparison between the stress-rupture behaviour of γ TiAl and Ti834. It is clear that γ TiAl offers significant improvements over Ti834, with a temperature benefit of approximately 75-100°C. Besides, recent comprehensive

studies by Abdallah et al [29] also demonstrated that the γ TiAl showed enhanced improvements of ~ 250MPa in terms of strength. Alongside the ductility measurements for γ TiAl described previously, this clearly offers encouragement for designers looking to take advantage of the weight savings that a range of titanium aluminides can provide.

The superior high temperature creep behaviour of γ TiAl over Ti834 is partly due to the reduction in environmental damage. A characteristic of the creep behaviour of Ti834 at temperatures in excess of 625°C is the severe oxidation, known as α-case formation, and subsequent brittle cracking at the surface [30-32], as shown in Figure 16 (a) and (b), respectively. It has been reported [30-33] that the existence of this brittle oxidised layer limits the creep capability of Ti834 particularly under high stress conditions, where a marked drop in ductility is observed, as shown in Figure 17. Ultimately, these differences in oxidation resistance are responsible for the similar levels of ductility measured in the two classes of material at the extremes of their performance window, i.e. creep ductility in Ti834 is essentially restricted by the α case formation and cracking [34].

The ability to accurately predict the creep behaviour of modern alloys such as γ TiAl is critical to design engineers. Although in service component failures will usually be fatigue dominated, accurate creep models are essential to the description of stress evolution in support of finite element approaches which seek to predict fatigue failure. As such it is relevant to compare traditional techniques such as the Larson-Miller approach to more modern lifing methods including the Wilshire equations and the hyperbolic tangent method. A comparison of the techniques in terms of stress-rupture, Figures 8-10, shows that both the Wilshire equations and the hyperbolic tangent method show improved curve fits when compared to Larson-Miller technique. In particular the sigmoidal shape of the curves seems to be more representative of the data than that of the power law based Larson-Miller approach.

As stated previously, n values in excess of 4 would appear to indicate dislocation creep as the dominant mechanism in the creep deformation of Ti-45Al-2Mn-2Nb. The fact that the Wilshire equations in particular are capable of accurately representing all of the data, along with reasonably consistent elongation behaviour, Figure 13, supports the fact that no transition from dislocation to diffusional creep occurs. This is consistent with many previous applications of the Wilshire equations [8-11]. However, the Wilshire equations offer further insight into material behaviour with transitions within the bi-modal dataset related to physical phenomena, i.e. bulk yield within the material. Above the yield stress, dislocations are continually generated and creep occurs by movement of these dislocations. Extrapolation of this data to stress values below σ_y, however, leads to an overestimation of the creep rate and hence an underestimation of the actual rupture time. At stresses lower than this transition point, a second line is drawn which now represents the fact that creep occurs only by the movement of pre-existing dislocations in the structure, and a more shallow curve is observed for data at $\sigma<\sigma_y$. It is vital to mention that the transition points in these curves have been recently explored and experimentally verified in studies carried out by the same author based on creep data of Ti834 [34, 35].

Encouragement is also gained from the fact that the Wilshire equations accurately describe the minimum strain rate data for the material, and that the derived Q_c^* value compares favourably with the activation energy for self diffusion in the titanium lattice [34]. With the ability to relate these observations from the Wilshire equation approach to physical phenomena, confidence is gained that extrapolation outside of the current stress-rupture time space should provide representative results.

5. Conclusions

- Accurate representation of the creep behaviour of Ti-45Al-2Mn-2Nb can be achieved through modern creep lifing techniques such as the Wilshire equations and Hyperbolic Tangent methods.
- Values of Q_c* derived from the Wilshire equations correlate to physical phenomena such as the yield stress and activation energy for self diffusion in the material.
- When compared to the conventional titanium alloy Ti834, the intermetallic Ti-45Al-2Mn-2Nb demonstrated significant improvements in temperature capability for creep (75-100°C improvement) for a given stress condition.
- The ductility measurements in the alloy Ti-45Al-2Mn-2Nb were encouraging, consistently exceeding 15% over the range of conditions assessed.
- The alloy Ti-45Al-2Mn-2Nb showed a superior resistance to surface oxidation (α case formation) and cracking compared to Ti834.

Acknowledgments

The current research was conducted under the Technology Strategy Board (TSB) contract SILOET (AB266C/4). The financial and technical support from TSB and Rolls-Royce plc is acknowledged.

References

[1] Austin C. Curr. Opin. Solid State Mater. Sci. 1999; 4: 239-242.

[2] McBride J, Malinov S, Sha W. Mater. Sci. Eng. A 2004; 384: 129-137.

[3] Young-Won Kim. Mater. Sci. Eng. A 1995; 192/193: 519-533.

[4] Djanarthany S, Viala J, Bouix J. Mater. Chem. Phys. 2001; 72: 301-319.

[5] Kerry S, Winstone M. Mater. Sci. Eng. A 1995; 192/ 193: 856-861.

[6] Soboyejo W, Mercer C, Lou K, Heath S. Metall. Mater. Trans. A 1995; 26: 2275-2291.

[7] Bache MR, Bradshaw C, W Voice. Mater. Sci. Eng. A 2003; 354: 199-206.

[8] Wilshire B, Battenbough A. Mater. Sci. Eng. A 2007; 443: 156-166.

[9] Wilshire B, P Scharning. Scr. Mater. 2007; 56: 701-704.

[10] Wilshire B, Scharning P. Int. Mater. Rev. 2008; 53: 91-104.

[11] Wilshire B, Scharning P. Mater. Sci. Tech. 2008; 24: 1-9.

[12] Prasad U, Chaturvedi M. Metall. Mater. Trans. A 2003; 34: 2053-2066.

[13] Diologent F, Kruml T. Mater. Sci. Eng. A 2008; 487: 377-382.

[14] Wilshire B, Evans RW, Introduction to Creep: The institute of Materials; London; UK; 1993.

[15] Retina V, Ahlstrom J, Karlsson B. Mater. Charact. 1997; 38: 287-300.

[16] Wilshire B, Whittaker MT. Acta Mater. 2009; 57: 4115-4124.

[17] Brown S, Evans RW, Wilshire B. Mater. Sci. Eng. 1986; 84: 147-156.

[18] Monkman F, Grant N. Proc. ASTM 1956; 56: 593-620.

[19] Williams S. Report MFR30017: Rolls-Royce plc; Derby; UK, 1993.

[20] Williams S, Compass 1999: Proc. 1st Int. Conf. on Compon. Optim.; Swansea; UK; 1999: 139-146.

[21] Williams S, Bache MR, Wilshire B. Mater. Sci. Tech. 2010; 26: 1332-1337.

[22] Larson F, Miller J. Trans. ASME 1952; 74: 765-775.

[23] Wilshire B, Scharning P, Hurst R. Energy Mater.: Mater. Sci. Eng. Energy Syst. 2007; 2: 84-88.

[24] Bartolotta P, Krause D. Report NASA/TM-1999-209071; Glenn Research Centre; Ohio, USA; 1999.

[25] Han C, Park N, Song B, Hong W. Microelectron. Packag. Conf.; Rimini; Italy; 2009: 1-4.

[26] Langdon T. Metall. Mater. Trans. A 2002; 33: 249-259.

[27] Parthasarathy T, Mendiratta M, Dimiduk D. Scr. Mater. 1997; 37: 315-321.

[28] Chen W, Triantafillou J, Beddoes J, Zhao L. Intermet. 1999; 7: 171-178

[29] Abdallah Z, Dixon M, Whittaker MT, Bache MR. Proc. CREEP 2012 Conf.; Kyoto; Japan; 2012.

[30] Evans RW, Hull R, Wilshire B. J Mater. Process. Tech. 1996; 56: 492-501.

[31] Evans RW, Hull R, Wilshire B. The 8th Int. Conf. Fract. (ICF8); Kiev; Ukraine; 1993: 521-528.

[32] Abdallah Z, Perkins K, Williams S. Metall. Mater. Trans. A 2012; In Press; DOI: 10.1007/s11661-012-1285-3.

[33] Gurappa I. J Mater. Sci. Lett. 2003; 22: 771-774.

[34] Abdallah Z. PhD Thesis; Rolls-Royce/University Technology Centre (UTC) - Swansea University; 2010.

[35] Abdallah Z, Perkins K, Williams S. Mater. Sci. Eng. A 2012; 550: 176-182.

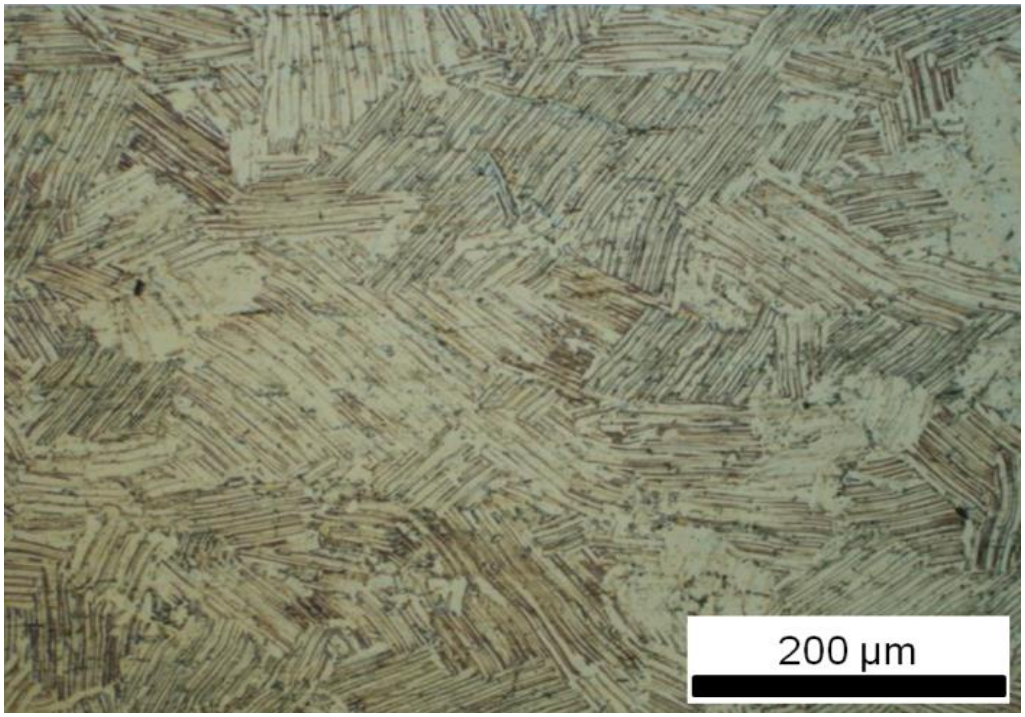

Figure 1: Microstructure of the cast and HIP'ed Ti-45Al-2Mn-2Nb

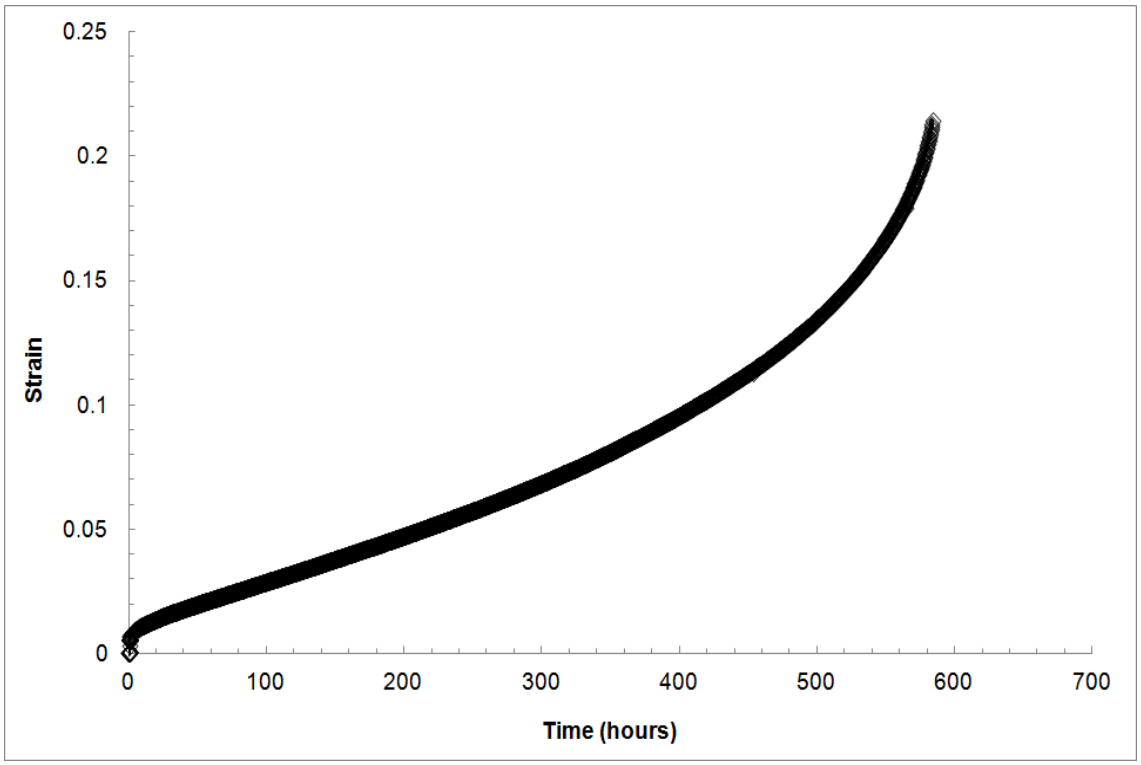

Figure 2: A typical strain-time (creep) curve for Ti-45Al-2Mn-2Nb, at 675^{o}C and 450MPa showing primary, secondary and tertiary stages.

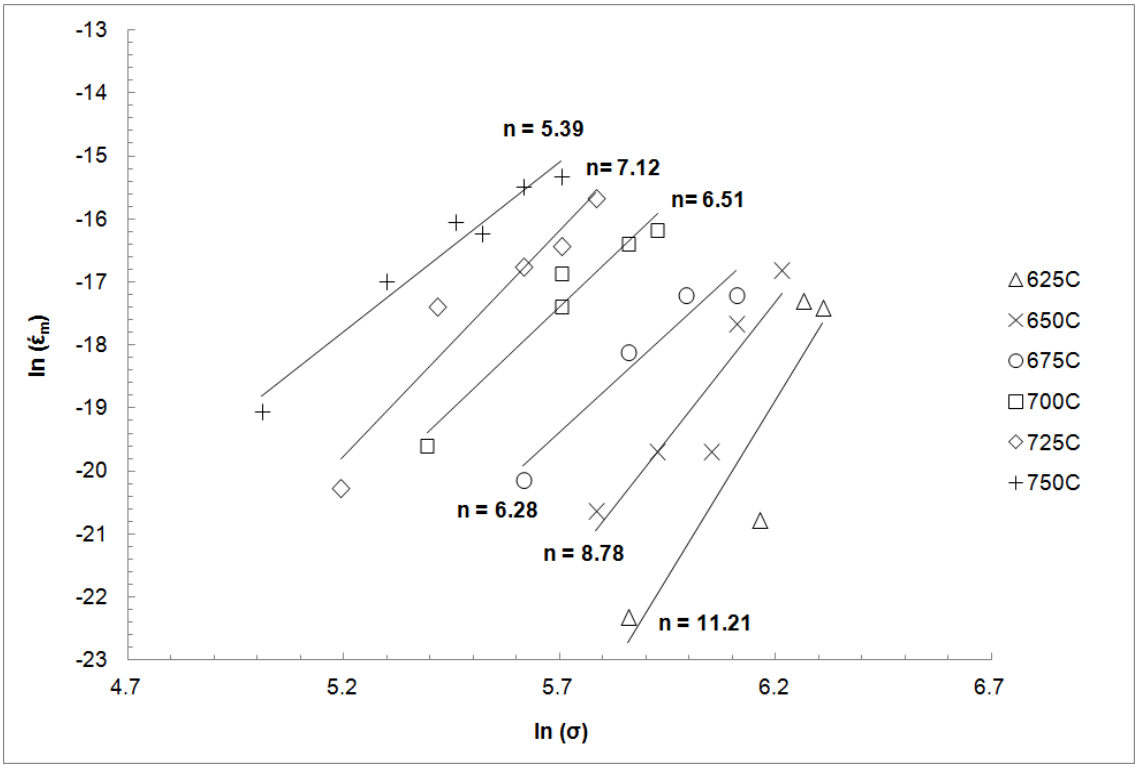

Figure 3: The relationship between (ln $\dot{\varepsilon}_m$) and (ln σ), at constant temperatures, where the slope represents the value of the stress exponent n.

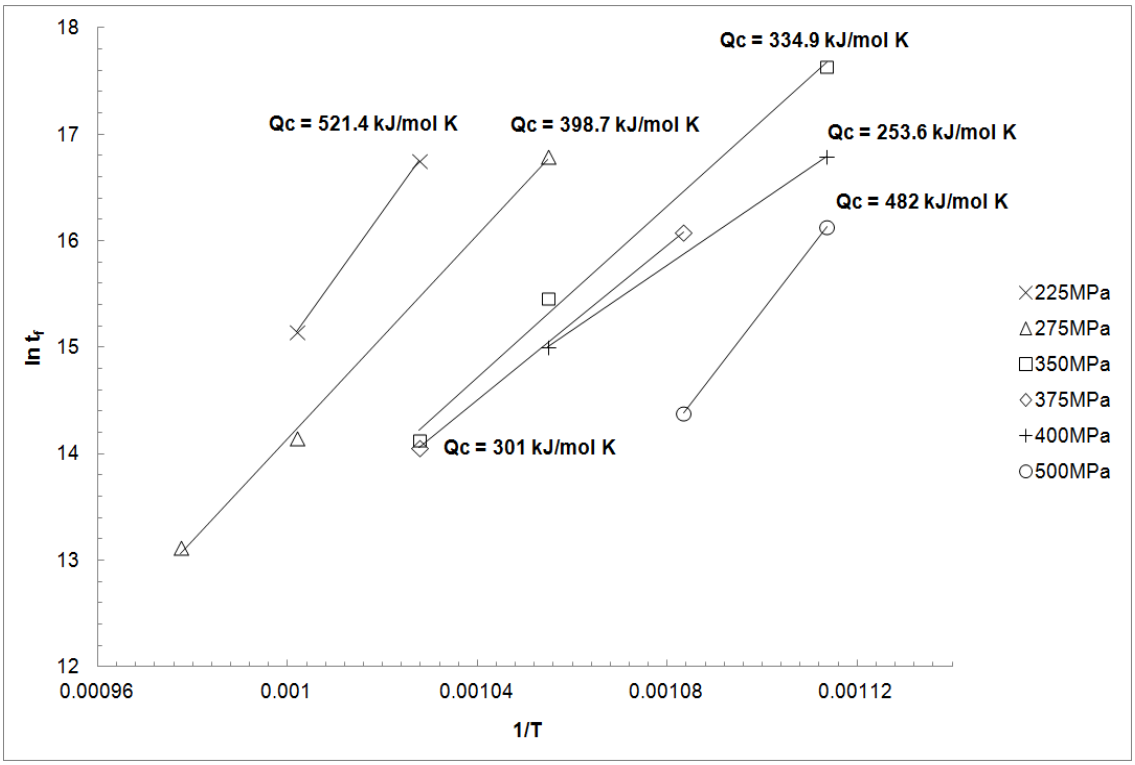

Figure 4: The relationship between (ln t_f) and (1/T), at constant stresses. The slope of the lines represents the value of Qc/R from which Qc can be calculated (R = 8.314 J/mol K).

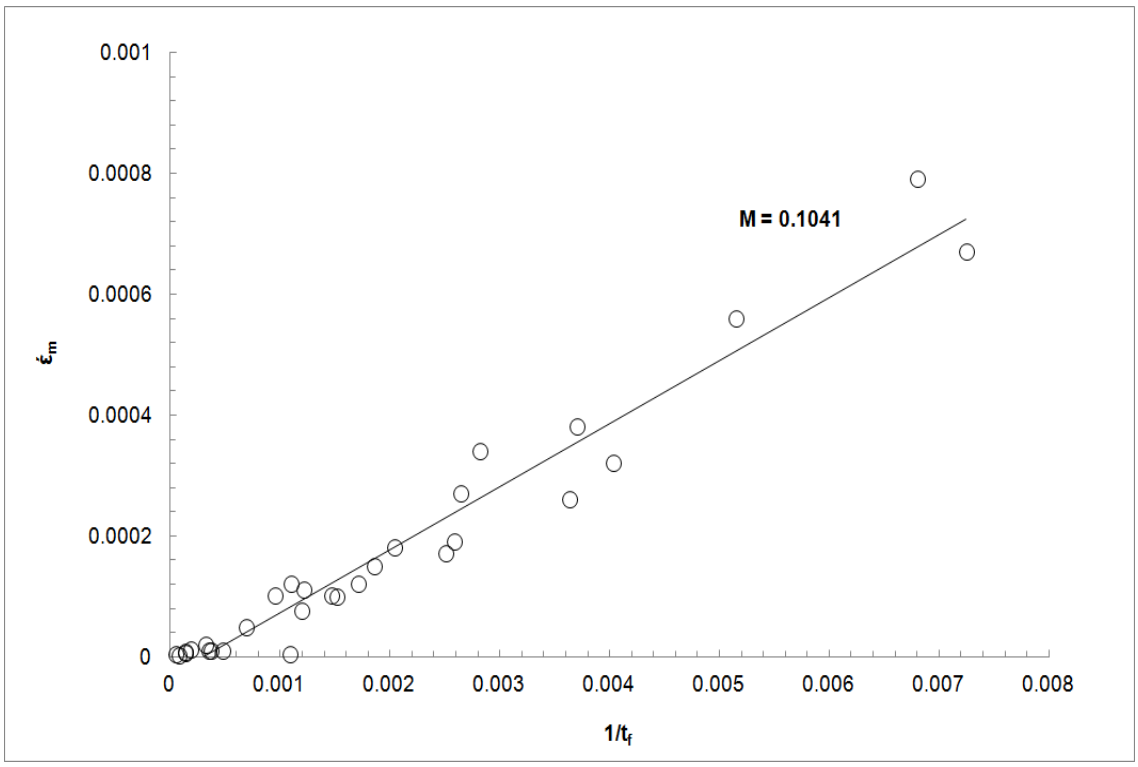

Figure 5: The relationship between the minimum creep rate, $\dot{\varepsilon}_m$, and the inverse of the time to fracture, $1/t_f$, according to the Monkman-Grant relationship. The slope is the value of the Monkman-Grant constant, M.

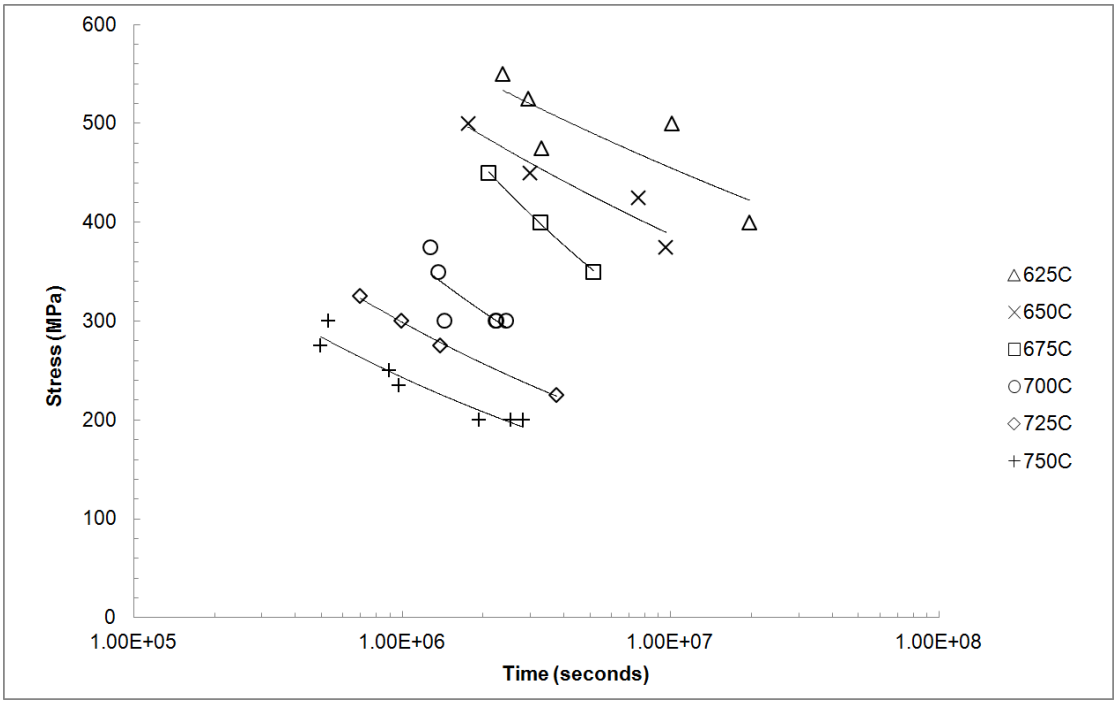

Figure 6: The stress rupture data at various temperatures fitted using least square methods.

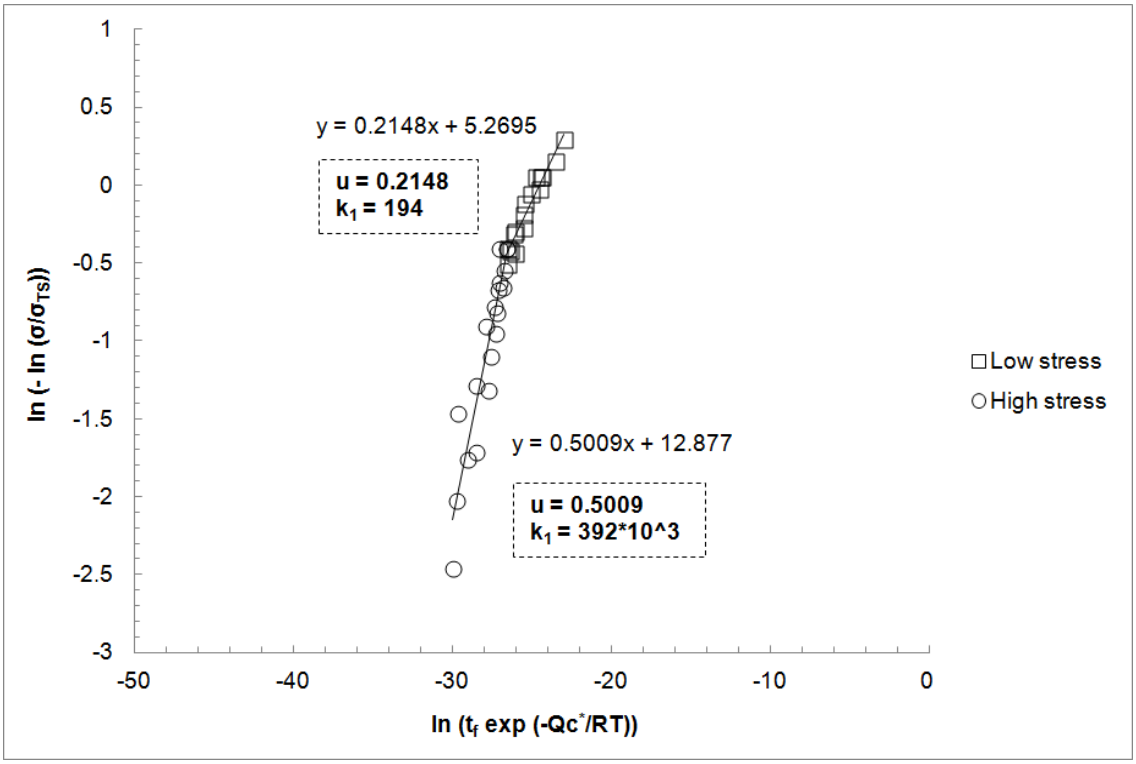

Figure 7: Calculating the value of the constants u and k_1 by plotting ln (- ln (σ/σ_{TS})) against ln (t_f exp (-Qc^*/RT)).

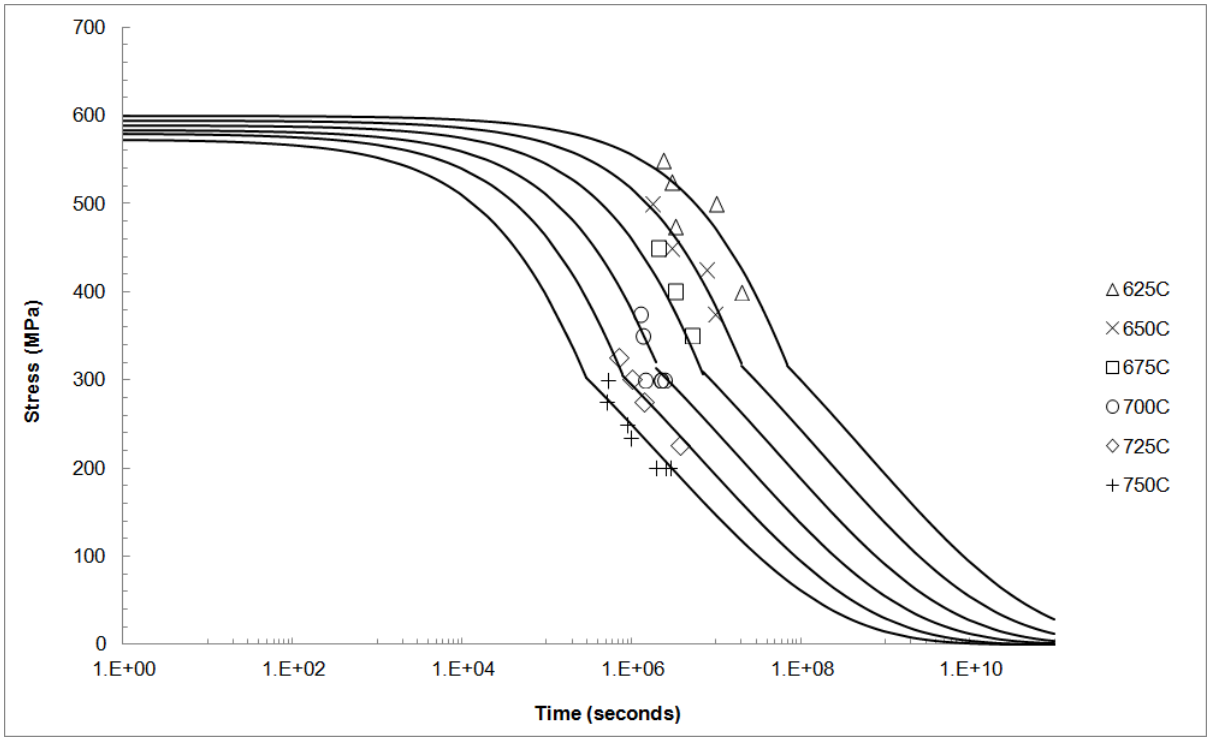

Figure 8: The predictive creep rupture curves obtained using the Wilshire technique (equation 3) superimposed on the experimental creep data.

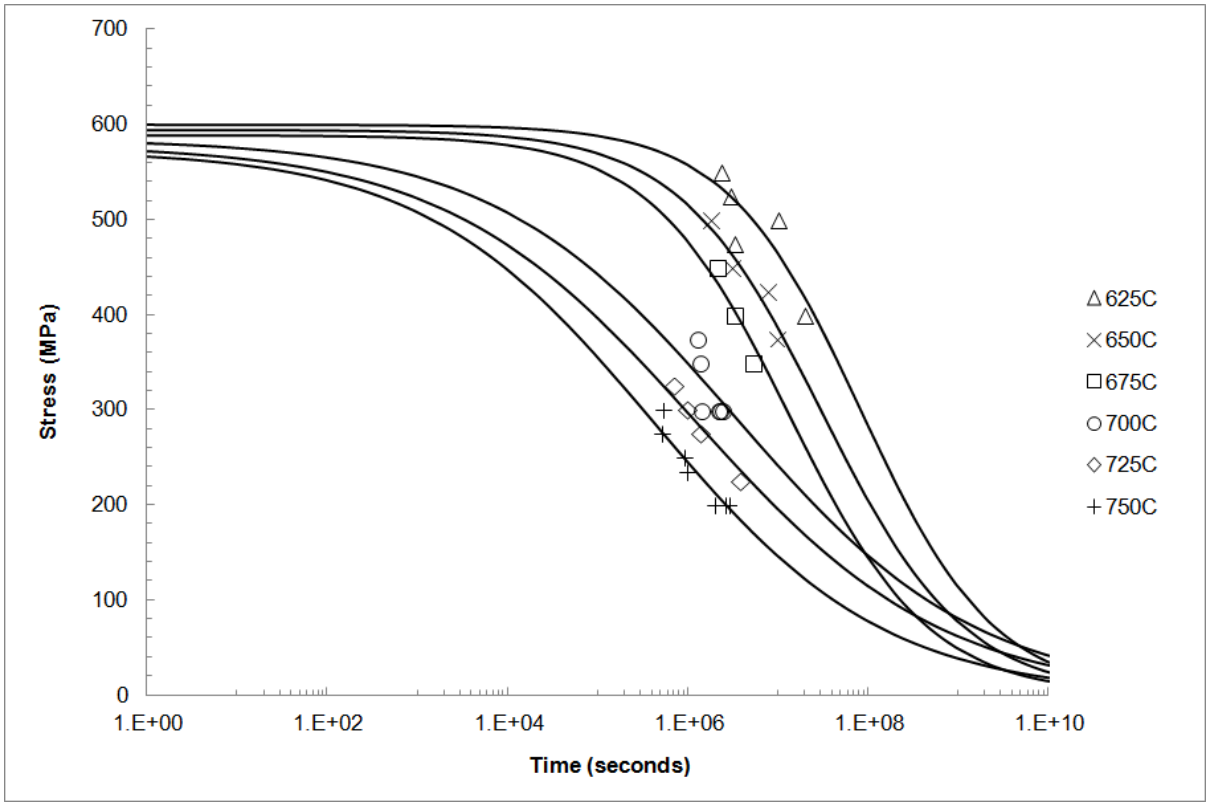

Figure 9: The predictive creep rupture curves obtained using the Hyperbolic Tangent technique (equation 4) superimposed on the experimental creep data

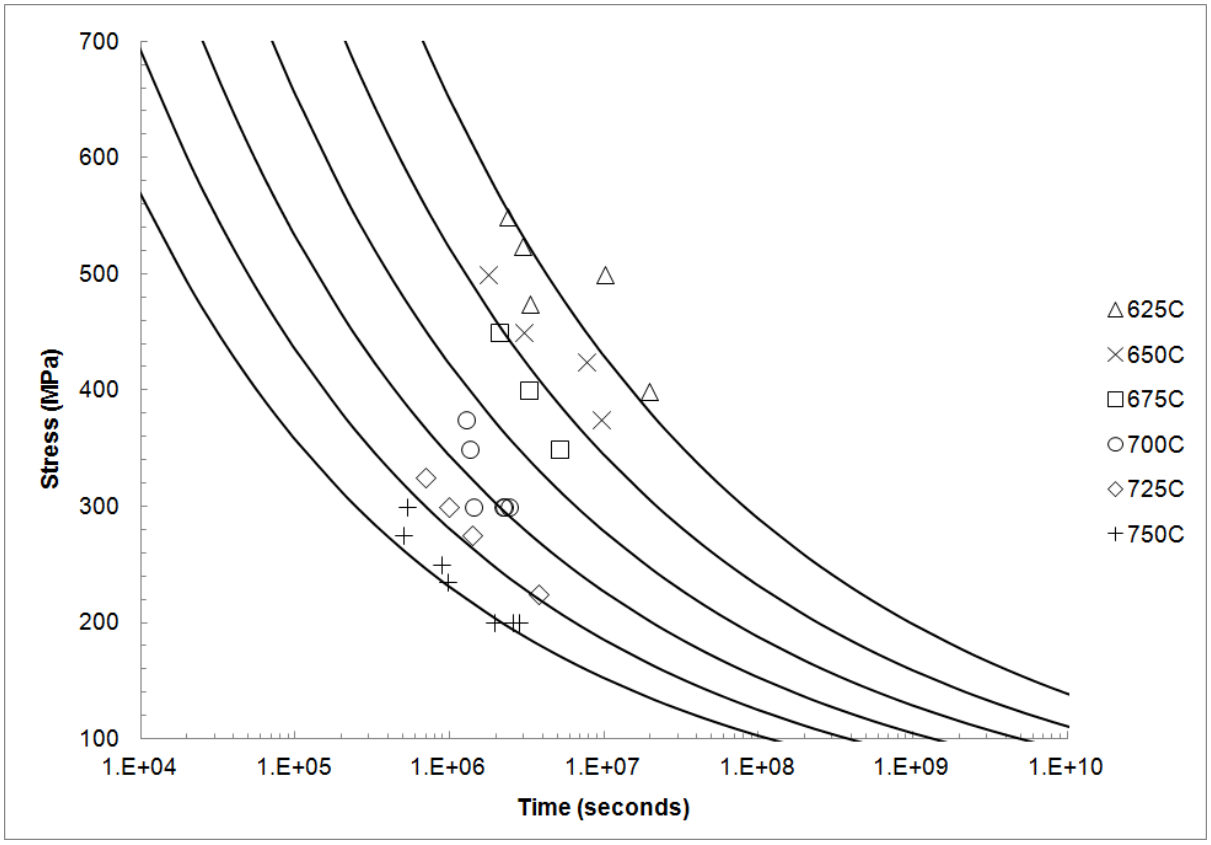

Figure 10: The predictive creep rupture curves obtained using the Larson-Miller technique (equation 5) superimposed on the experimental creep data.

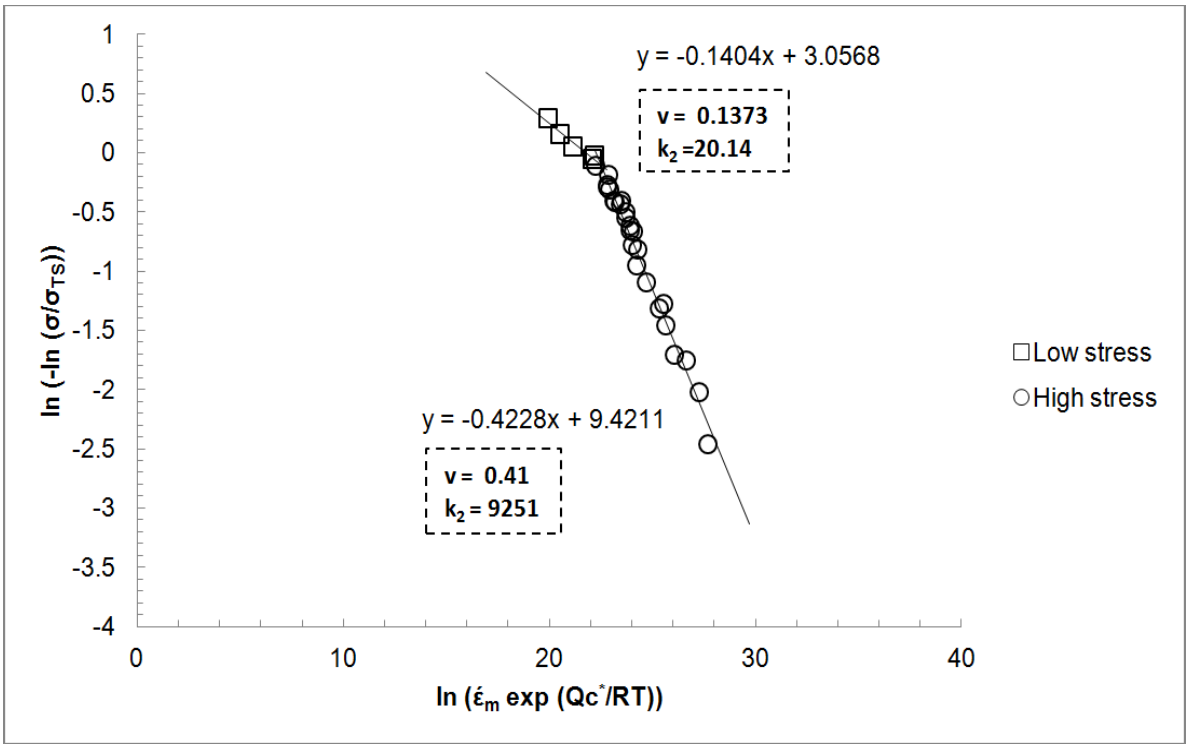

Figure 11: Calculating the value of the constants v and k_2 by plotting ln (- ln (σ/σ_{TS})) against ln ($\acute{\varepsilon}_m$ exp (Qc^*/RT)).

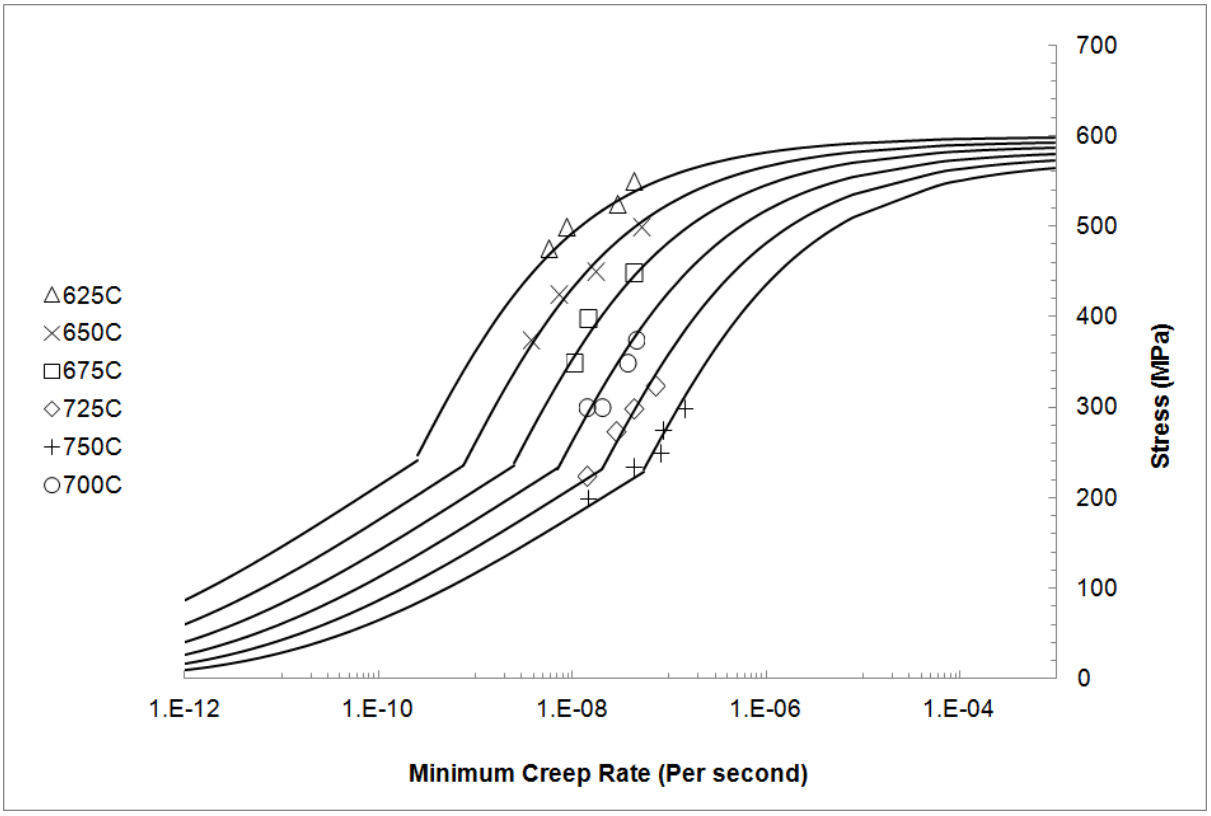

Figure 12: The minimum creep rate prediction curves obtained using the Wilshire technique (equation 6) superimposed on the actual creep data.

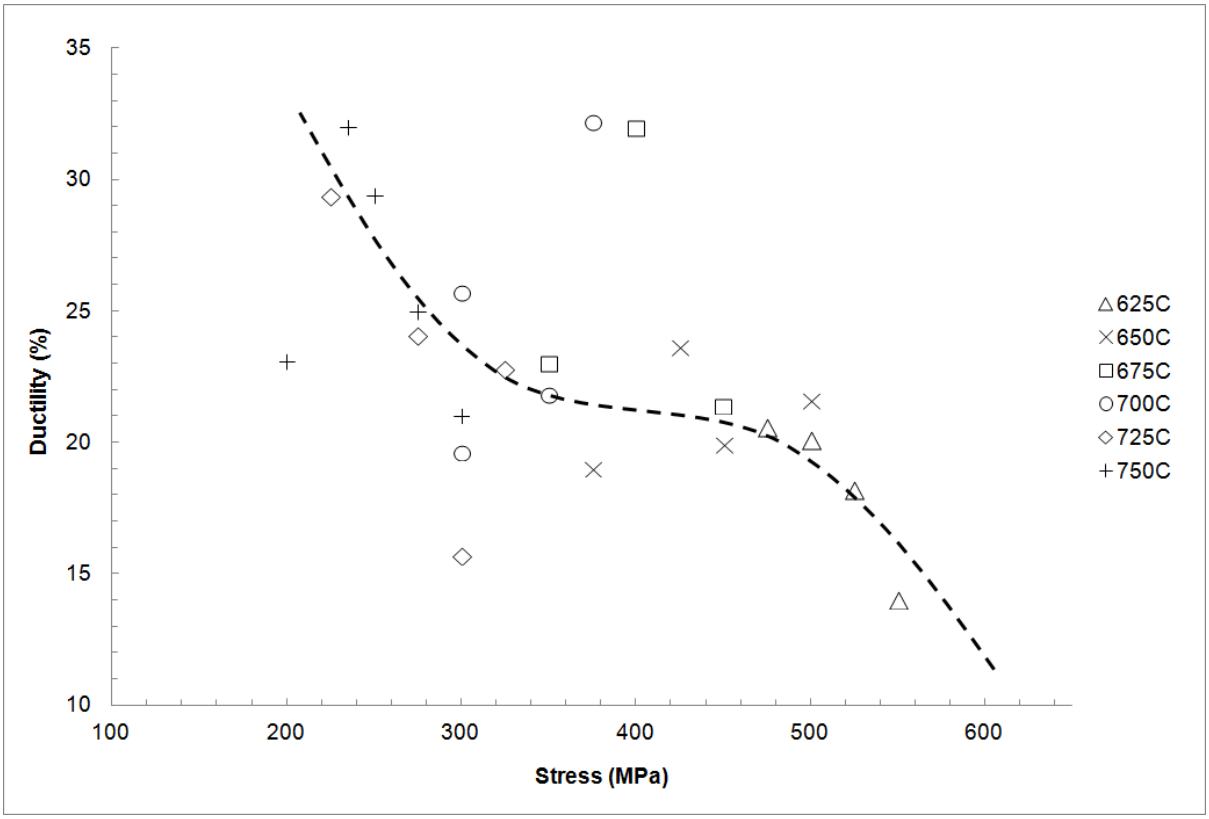

Figure 13: The measured creep ductility versus stress at all test temperatures for Ti-45Al-2Mn-2Nb.

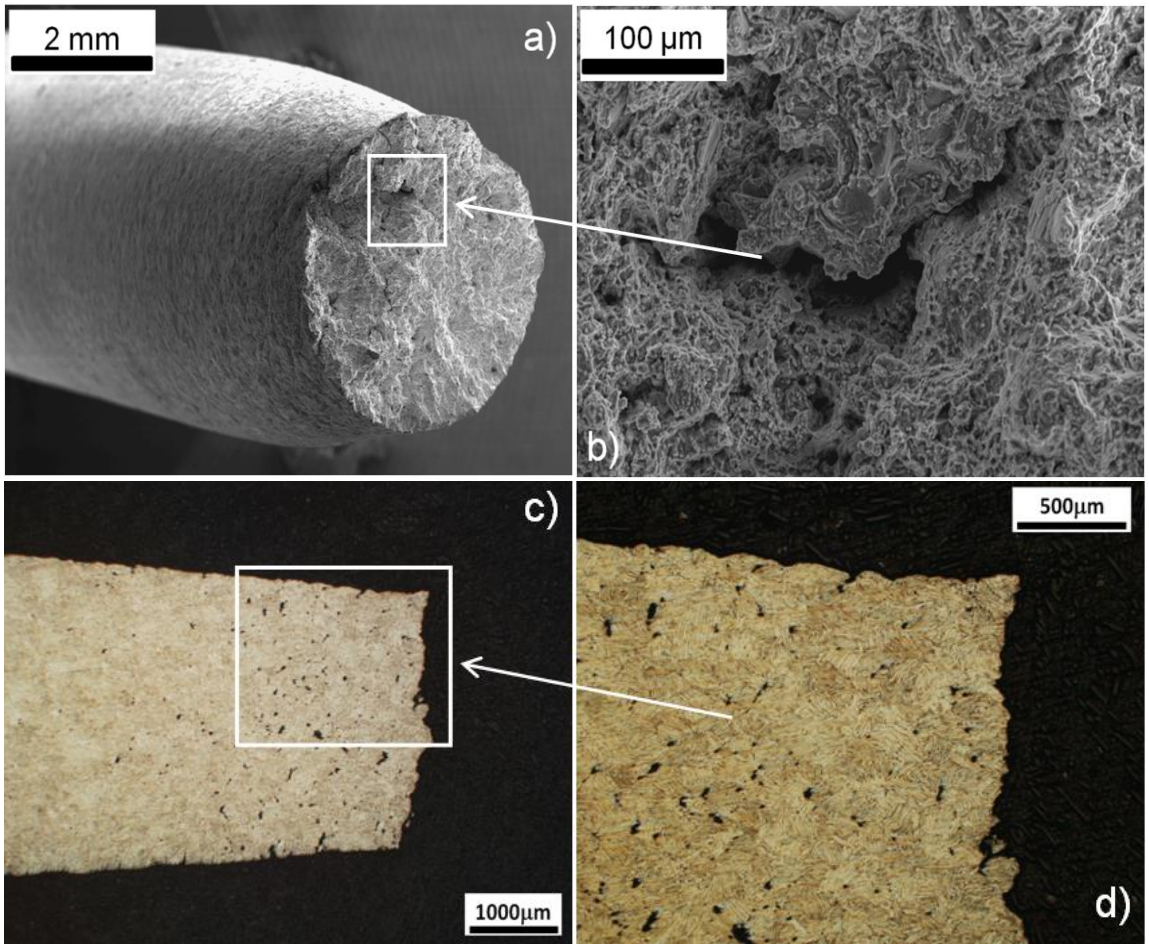

Figure 14: A crept Ti-45Al-2Mn-2Nb specimen at 725^{o}C/275MPa: a) An SEM image showing intergranualr cracking, b) a highly magnified image of (a), c) a longitudinal section of the crept specimen showing internal voids and interlamellar cracking, d) a highly magnified optical image showing voids at the interlamellar interfaces.

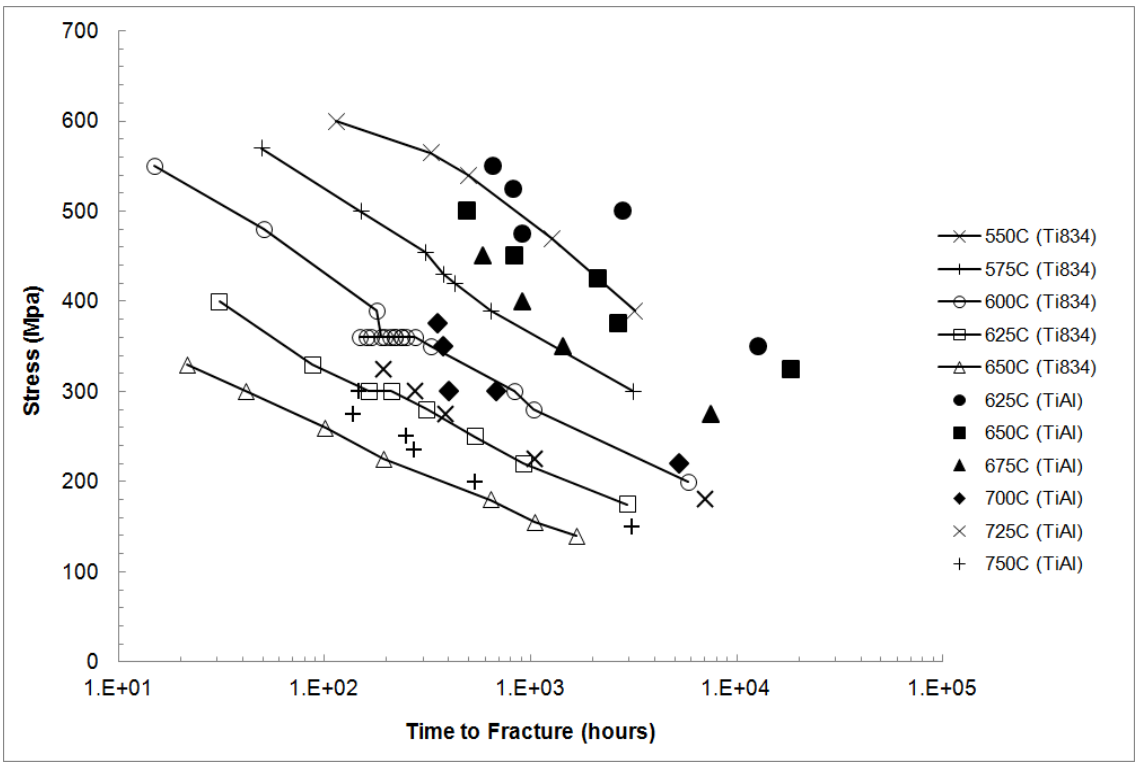

Figure 15: Stress-rupture behaviour recorded at different temperatures for Ti-45Al-2Mn-2Nb and Ti 834.

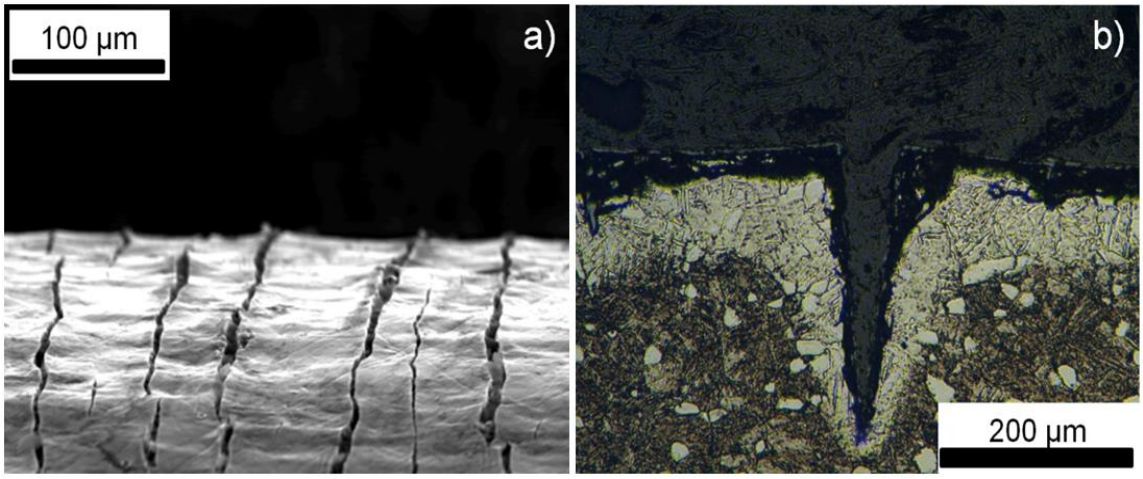

Figure 16: a) An oxidised and cracked specimen surface and, b) longitudinal section displaying α case cracking for a Ti834 specimen tested at 650°C/140MPa. No such oxidation damage is observed in Ti-45Al-2Mn-2Nb.

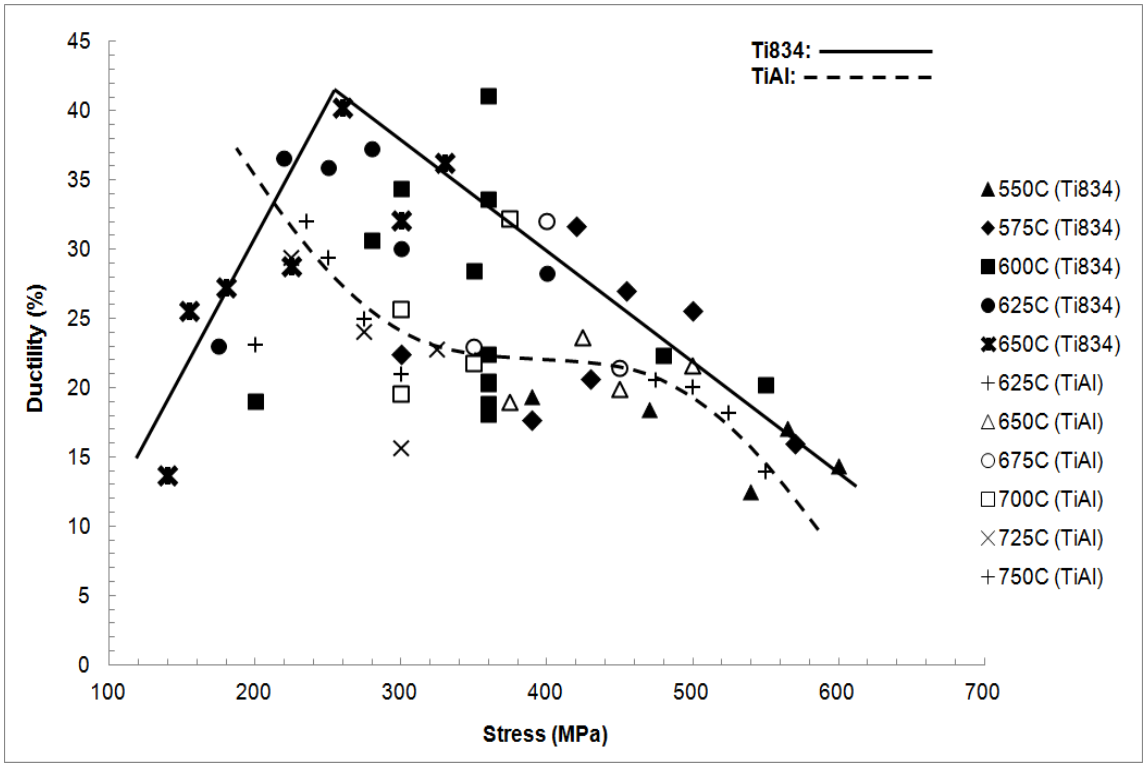

Figure 17: The measured creep ductility versus stress at all test temperatures for Ti-45Al-2Mn-2Nb compared to those for Ti 834.